SUPPLEMENTARY APPENDIX

Platelet glycoprotein VI and C-type lectin-like receptor 2 deficiency accelerates wound healing by impairing vascular integrity in mice

Surasak Wichaiyo,[1,2] Sian Lax,[1] Samantha J. Montague,[1] Zhi Li,[3] Beata Grygielska,[1] Jeremy A. Pike,[4] Elizabeth J. Haining,[1] Alexander Brill,[1,5] Steve P. Watson,[1,4,6] and Julie Rayes[1]

[1]Institute of Cardiovascular Sciences, College of Medical and Dental Sciences, University of Birmingham, Birmingham, UK; [2]Department of Pharmacology, Faculty of Pharmacy, Mahidol University, Bangkok, Thailand; [3]Institute of Immunology and Immunotherapy, College of Medical and Dental Sciences, University of Birmingham, Birmingham, UK; [4]Centre of Membrane Proteins and Receptors (COMPARE), Universities of Birmingham and Nottingham, The Midlands, UK; [5]Department of Pathophysiology, Sechenov First Moscow State Medical University, Moscow, Russia and [6]Institute of Microbiology and Infection, College of Medical and Dental Sciences, University of Birmingham, Birmingham, UK

 doi:10.3324/haematol.2018.208363

Received: October 12, 2018.

Accepted: January 28, 2019.

Pre-published: February 7, 2019.

Correspondence: *JULIE RAYES* - j.rayes@bham.ac.uk

STEVE P. WATSON - s.p.watson@bham.ac.uk

Supplemental materials

Supplemental methods:

Animal

In this study, C57BL/6 mice were bred to produce wild type (WT) and platelet-specific CLEC-2-deficient (*Clec1b*$^{fl/fl}$*Pf4-Cre*)[1] mice as littermates separately from GPVI knockout (*Gp6*$^{-/-}$)[2] and CLEC-2/GPVI double-deficient (*Clec1b*$^{fl/fl}$*Pf4-Cre/Gp6*$^{-/-}$; DKO) mice. Additionally, *Clec1b*$^{fl/fl}$*Pf4-Cre* mice were used for breeding in the DKO producing colony. Cross comparisons were made between related, age- and sex-matched animals to control natural variation between mouse strains, including between WT and DKO mice.

Morphometric analysis

Wounds were excised, fixed in 4% paraformaldehyde and processed using a standard paraffin embedding protocol. Paraffin-embedded skin samples (5 μm) were used for hematoxylin and eosin (H&E) staining. Tissues were imaged using a ZEISS AxioScan.Z1 slide scanner. As shown in the scheme below, the proliferation of keratinocytes forms the hyperplastic epidermis (He) at the wound edge within a few days after injury. The granulation tissue, containing newly formed blood vessels, infiltrating cells, and molecules, is also formed to facilitate wound healing. Keratinocytes migrate underneath the scab and above the granulation tissue, which generate epithelial tongues toward the centre of the wound to resurface skin epidermis (the tips of epithelial tongue are indicated by red arrow).[3-5] Morphometric analysis of skin histology was performed manually using a freehand line tool in Fiji (a distribution of ImageJ software)[6], and the terms were defined in the following ways;

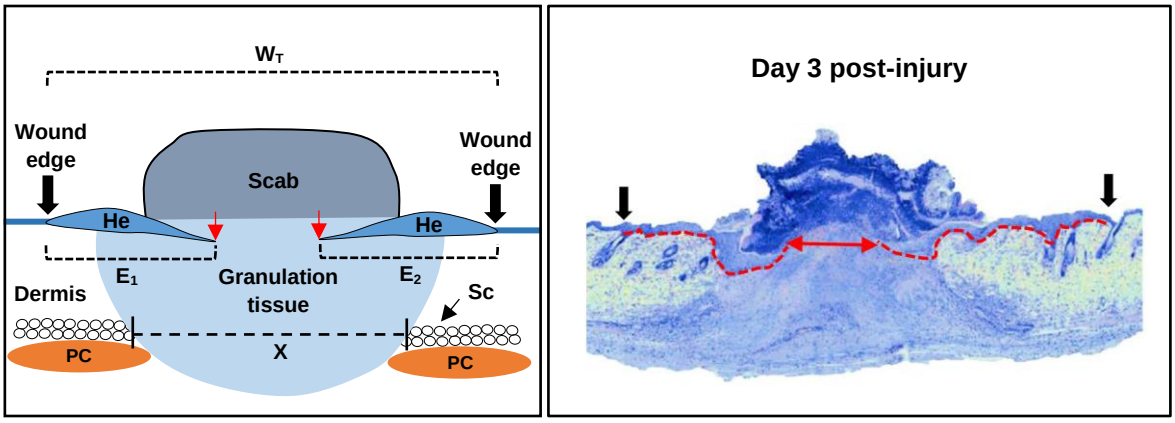

- Re-epithelialization is the re-generation of skin epidermis.[7,8] The area of thickening keratinocytes immediately next to the normal skin in histology images is considered as the wound edge for measuring re-epithelialization.[8-13] Percentage of re-epithelialization at day 3 post-injury was calculated using the formula[8,9];

$$\% \text{ Re-epithelialization} = [(E_1+E_2)/W_0] \times 100$$

where E_1 and E_2 = distance of epithelial tongue from each side of wound edge

W_0 = original wound diameter at day 0

- Wound contraction, which is mediated by the specialized muscle called "*panniculus carnosus* (PC)" in deeper layer of murine skin, also affects wound closure.[14] To exclude the influence of this effect, closure by contraction at day 3 post-injury was calculated using the formula[9];

$$\% \text{ Wound contraction} = [(W_0-W_T)/W_0] \times 100$$

where W_T = distance between the wound edges at indicated time point

- The area of granulation tissue, which contributes to new tissue re-formation, was also measured at day 3 post-injury.[4,5]
- Following the complete wound closure, thickened layer of keratinocytes is remained, known as scar. Thus, the length of hyperplastic epidermis ("a" in Figure 2C), which indicates the size of scar at upper layer, was examined at day 9 post-injury.[5,15]
- Measurement of distance between intact subcutaneous (Sc) edges at both side of the wound ("X" in above scheme and "b" in Figure 2C), which represents the size of scar in the deeper layer, was also performed at day 9 post-injury.[5]

Measurement of fibrin and collagen contents

Martius scarlet blue staining (Atom Scientific, UK) was used to detect fibrin and collagen. High power field (HPF) images were taken from the whole wound area. To calculate the mean intensity, the fibrin (red color) and collagen signals (blue color) were isolated using the Fiji Colour Deconvolution plugin (Masson Trichrome)[16] and the threshold set using the Otsu method[17]. A total intensity was normalized by total measured area, and expressed as fold relative to WT.

Immunohistochemistry and immunofluorescence

Immunohistochemistry staining for Gr-1, Ly6C, F4/80, fibrinogen, tissue factor (TF), tumor necrosis factor (TNF)-α, platelet factor 4 (PF4), CXCL-1 and podoplanin were performed on paraffin-embedded skin section (5 μm) according to a standard protocol[18]; horseradish peroxidase (HRP)-conjugated secondary antibodies and ImpactDAB substrate (SK-4105, Vector Lab) were used for signal detection. HPF images were taken from the whole wound area. Brown color was separated using IHC toolbox in

Fiji then thresholded (Otsu). The binary images were processed by filling holes and a watershed transform to separate touching cells. Per cell measurements were calculated for all connected areas larger than 45 square microns. Gr-1$^+$, Ly6C$^+$ and F4/80$^+$ cells were counted and presented per HPF[19], while intensity of TF[20], TNF-α, PF4, and CXCL-1[21] were quantified and normalized by total measured area, then expressed as fold relative to wild-type (WT).

Immunofluorescence staining for neuron-glial antigen 2 (NG2), CD41, podoplanin, vimentin, Ly6C, Ly6G, iNOS, Fizz-1, F4/80, and CD31 were processed in optimal cutting temperature compound (O.C.T)-embedded frozen skin sections (10 μm). Fluorophore-conjugated secondary antibodies were used to detect signals. Hoechst (H3570, Life Technologies) was used to stain nuclei. HPF images were taken from the whole wound area. CD31$^+$ area[22] was calculated using Otsu thresholding (Fiji) and normalized by total measured area, and presented as fold relative to WT. The iNOS$^+$F4/80$^+$ cells and Fizz-1$^+$F4/80$^+$ cells were counted using Fiji according to the previous protocol[23] with adaptation. In brief, HPF image of either iNOS$^+$F4/80$^+$ or Fizz-1$^+$F4/80$^+$ double staining was split into a single blue (nuclei), green (F4/80) and red (iNOS or Fizz-1) channel, respectively. The threshold of green fluorescence was set using Otsu model. Then, the binary images were processed by a watershed to separate attached particles. The red fluorescence was also thresholded. To create a merged image of previously processed red and green channels, the “image calculator” mode from process menu was used, followed by choosing the operator “AND”. Finally, all connected areas larger than 45 square microns were counted as per cell measurements. The antibodies used are described in Table S1.

In vitro neutrophil migration assay

Neutrophils were isolated from the bone marrow of WT or DKO mice as previously described[24] and purity was checked using anti-Ly6G antibody. Isolated neutrophils (50,000 cells diluted in Hank's Balanced Salt Solution + 0.5 % bovine serum albumin) were loaded into the upper well of a chemotaxis chip (Ibidis). The chemotaxis chips were coated with collagen (10µg/ml), fibrinogen (100 µg/ml) or crosslinked fibrin (prepared by mixing fibrinogen (1 mg/ml), thrombin (1 U/ml), Ca^{2+} (10 mM), and FXIIIa (7 µg/ml) in PBS for 1 hour at 37 °C). Chemotaxis toward fMLP (5 µM, Sigma) was assessed for 3 hours. After fixation with formalin, the cells in the loaded and migrated wells were imaged, and the number of cells in five representative areas per sample was quantified using Fiji. Finally, percentage of migrated cells was calculated using the formula;

$$\text{Percent neutrophil migration} = [N1/(N1+N2)] \times 100$$

Where N1 = numbers of migrated cells, N2 = numbers of remaining cells in loaded chamber

Hematological analysis

Whole blood was collected from the inferior vena cava using ethylenediaminetetraacetic acid (EDTA)-filled syringe. Blood counts were analyzed on an ABX Pentra 60 (Horbia Ltd, UK).

Statistical analysis

All data are presented as mean ± standard error of mean (SEM). Two-way ANOVA with Bonferroni's multiple comparison test was used to compare kinetics of wound closure. Mean differences in other parameters were analyzed by either Student's t-test (two groups comparison) or one-way ANOVA with Bonferroni post-hoc test (more than two groups) using GraphPad Prism software. $p<0.05$ was considered as statistically significant.

Table S1. List of antibodies used in immunostaining

Reagents	Working dilution	Company	Cat No.
Primary antibodies			
Rat anti-mouse Gr-1 monoclonal antibody	1:200	eBiosciences	14-5931-82
Rat anti-mouse F4/80 monoclonal antibody	1:200 (IHC) 1:100 (IF)	Bio-Rad	MCA497GA
Rabbit anti-mouse CXCL-1 monoclonal antibody	1:200	R&D systems	MAB4532
Syrian hamster anti-mouse podoplanin monoclonal antibody	1:500 (IHC) 1:200 (IF)	eBiosciences	14-5381-85
Rat anti-mouse CD41 monoclonal antibody	1:100	BD Pharmagen	553847
Rabbit anti-CD31 polyclonal antibody	1:100	Abcam	ab28364
Rabbit anti-NG2 chondroitin sulfate proteoglycan polyclonal antibody	1:200	Merk Millipore	AB5320
Rabbit anti-tissue factor monoclonal antibody	1:400	Abcam	ab151748
Rabbit anti-TNF alpha polyclonal antibody	1:200	Abcam	ab9739
Rat anti-mouse Ly6C monoclonal antibody	1:200	Biolegend	128002
Rat anti-mouse CXCL4/PF4 monoclonal antibody	1:200	R&D systems	MAB595-100
Goat anti-mouse fibrinogen polyclonal antibody	1:200	Accurate Chemical & Scientific Corp.	YNGMFBG7S
Rabbit anti-vimentin monoclonal antibody	1:200	R&D systems	MAB2105
Rabbit anti-iNOS polyclonal antibody	1:50	Abcam	ab15323
Rabbit anti-RELM alpha (Fizz-1) polyclonal antibody	1:50	Abcam	ab39626
Rat anti-mouse Ly6G-APC/Cy7-conjugated monoclonal antibody (clone 1A8)	1:100	BD Pharmagen	560600
IgG control			
Rat IgG2b control	1:400	Bio-Rad	MCA1125
Rat IgG1,K control	1:200	Biolegend	400402
Golden Syrian hamster IgG control	1:500 (IHC) 1:200 (IF)	eBiosciences	14-4914-85
Rabbit IgG control	1: 10,000	Life technologies	10500C
Secondary antibodies			
Goat anti-rat IgG-HRP	1:200 (Gr-1) 1:500 (F4/80)	Santa Cruz	sc-2032
Goat anti-hamster IgG-HRP	1:500	Santa Cruz	sc-2905
Donkey anti-rabbit IgG-HRP	1:200	GE Healthcare	NA934V
Donkey anti-goat IgG-HRP	1:500	Santa Cruz	Sc-2020
Goat anti-rat IgG-Alexa 568	1:200	Life technologies	A11077
Goat anti-rat IgG-Alexa 488	1:200 (vimentin) 1:100 (F4/80)	Life technologies	A11006
Goat anti-hamster IgG-Alexa 488	1:200	Life technologies	A21110
Goat anti-rabbit IgG-Alexa 647	1:200 1:100 (iNOS and Fizz-1)	Life technologies	A21245
Hoechst	1:10,000	Life technologies	H3570

IHC = Immunohistochemistry, IF = Immunofluorescence

References

1. Finney BA, Schweighoffer E, Navarro-Nunez L, et al. CLEC-2 and Syk in the megakaryocytic/platelet lineage are essential for development. Blood. 2012;119(7):1747-1756.
2. Kato K, Kanaji T, Russell S, et al. The contribution of glycoprotein VI to stable platelet adhesion and thrombus formation illustrated by targeted gene deletion. Blood. 2003;102(5):1701-1707.
3. Shaw TJ, Martin P. Wound repair at a glance. J Cell Sci. 2009;122(Pt 18):3209-3213.
4. Lucas T, Waisman A, Ranjan R, et al. Differential roles of macrophages in diverse phases of skin repair. J Immunol. 2010;184(7):3964-3977.
5. Yang HS, Shin J, Bhang SH, et al. Enhanced skin wound healing by a sustained release of growth factors contained in platelet-rich plasma. Exp Mol Med. 2011;43(11):622-629.
6. Schindelin J, Arganda-Carreras I, Frise E, et al. Fiji: an open-source platform for biological-image analysis. Nat Methods. 2012;9(7):676-682.
7. Ben Amar M, Wu M. Re-epithelialization: advancing epithelium frontier during wound healing. J R Soc Interface. 2014;11(93):20131038.
8. Stavrou EX, Fang C, Bane KL, et al. Factor XII and uPAR upregulate neutrophil functions to influence wound healing. J Clin Invest. 2018;128(3):944-959.
9. Chen L, Mirza R, Kwon Y, DiPietro LA, Koh TJ. The murine excisional wound model: Contraction revisited. Wound Repair Regen. 2015;23(6):874-877.
10. Oda Y, Hu L, Nguyen T, Fong C, Tu CL, Bikle DD. Combined Deletion of the Vitamin D Receptor and Calcium-Sensing Receptor Delays Wound Re-epithelialization. Endocrinology. 2017;158(6):1929-1938.
11. Sheets AR, Demidova-Rice TN, Shi L, Ronfard V, Grover KV, Herman IM. Identification and Characterization of Novel Matrix-Derived Bioactive Peptides: A Role for Collagenase from Santyl(R) Ointment in Post-Debridement Wound Healing? PLoS One. 2016;11(7):e0159598.
12. Carretero M, Escamez MJ, Garcia M, et al. In vitro and in vivo wound healing-promoting activities of human cathelicidin LL-37. J Invest Dermatol. 2008;128(1):223-236.
13. Schmidt BA, Horsley V. Intradermal adipocytes mediate fibroblast recruitment during skin wound healing. Development. 2013;140(7):1517-1527.

14. Davidson JM, Yu F, Opalenik SR. Splinting Strategies to Overcome Confounding Wound Contraction in Experimental Animal Models. Adv Wound Care (New Rochelle). 2013;2(4):142-148.
15. Rono B, Engelholm LH, Lund LR, Hald A. Gender affects skin wound healing in plasminogen deficient mice. PLoS One. 2013;8(3):e59942.
16. Ruifrok AC, Johnston DA. Quantification of histochemical staining by color deconvolution. Anal Quant Cytol Histol. 2001;23(4):291-299.
17. Luo TL, Eisenberg MC, Hayashi MAL, et al. A Sensitive Thresholding Method for Confocal Laser Scanning Microscope Image Stacks of Microbial Biofilms. Sci Rep. 2018;8(1):13013.
18. Ramos-Vara JA. Principles and Methods of Immunohistochemistry. Methods Mol Biol. 2017;1641:115-128.
19. Qiang L, Sample A, Liu H, Wu X, He YY. Epidermal SIRT1 regulates inflammation, cell migration, and wound healing. Sci Rep. 2017;7(1):14110.
20. Zhou J, May L, Liao P, Gross PL, Weitz JI. Inferior vena cava ligation rapidly induces tissue factor expression and venous thrombosis in rats. Arterioscler Thromb Vasc Biol. 2009;29(6):863-869.
21. Smith E, Prasad KM, Butcher M, et al. Blockade of interleukin-17A results in reduced atherosclerosis in apolipoprotein E-deficient mice. Circulation. 2010;121(15):1746-1755.
22. Uchiyama A, Yamada K, Ogino S, et al. MFG-E8 regulates angiogenesis in cutaneous wound healing. Am J Pathol. 2014;184(7):1981-1990.
23. Arqués O, Chicote I, Tenbaum S, Puig I, Palmer HG. Standardized Relative Quantification of Immunofluorescence Tissue Staining. Protocol Exchange 2012.
24. Swamydas M, Lionakis MS. Isolation, purification and labeling of mouse bone marrow neutrophils for functional studies and adoptive transfer experiments. J Vis Exp. 2013(77):e50586.

Supplemental Figures:

Figure S1

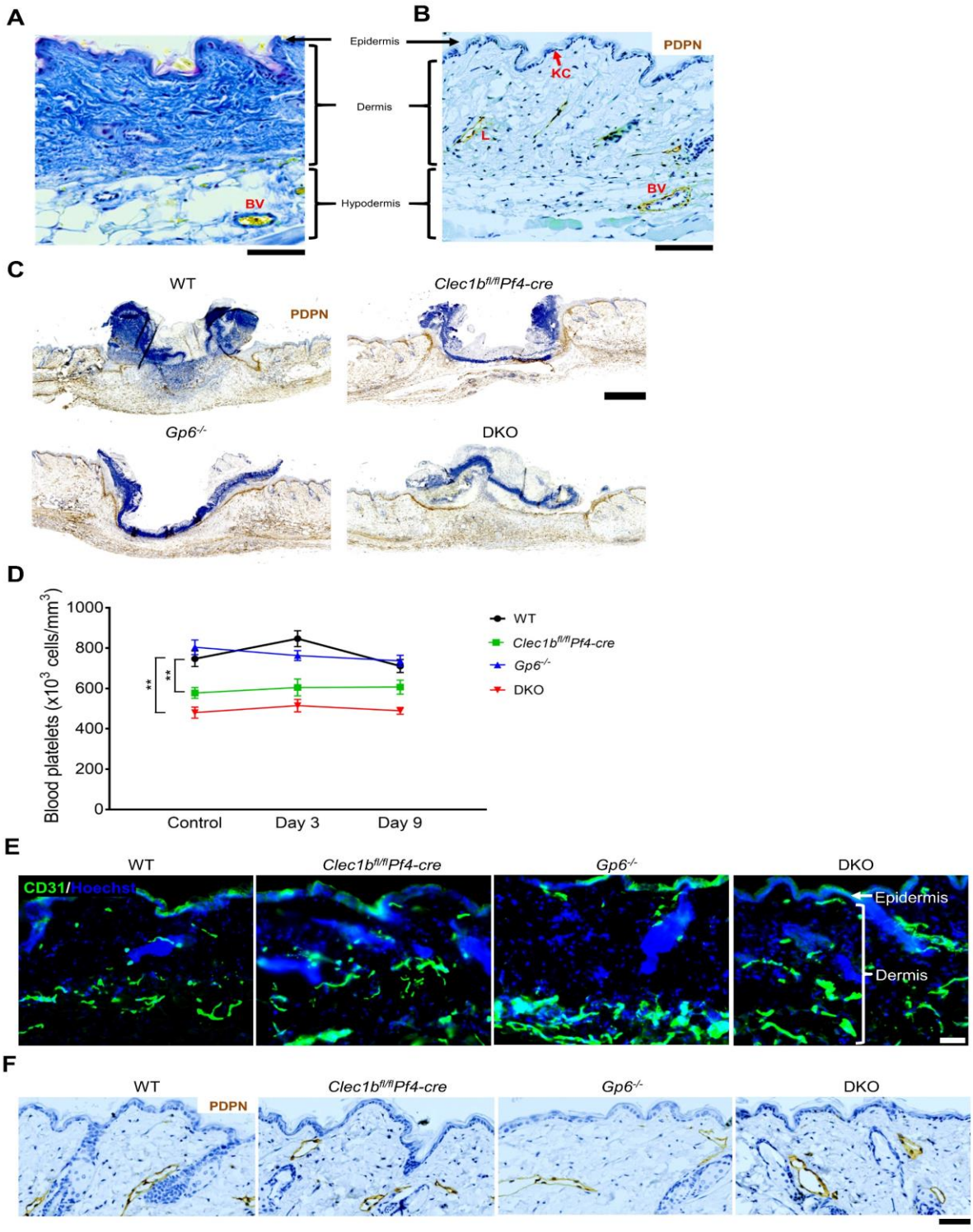

Figure S1. Platelet CLEC-2 deficient mice and DKO mice have lower baseline platelet counts than WT but no alteration in density of blood and lymphatic vessels in skin tissues. (A) Martius scarlet blue (MSB) staining shows collagen (blue) in dermis and hypodermis of unchallenged WT mouse skin (n=5). Red = old fibrin, blue = collagen, yellow = red blood cells/fresh fibrin. Scale bar = 100 μm. (B) Immunohistochemistry of podoplanin (brown) in unchallenged WT mouse skin (n=5). L = lymphatic vessel, KC = keratinocyte. PDPN = podoplanin. BV = blood vessel. Scale bar = 100 μm. (C) Podoplanin immunohistochemistry staining (brown) of skin wound at day 3 post-injury shows upregulation of podoplanin on migrating keratinocytes and on stromal and infiltrating cells within the granulation tissue in all groups (n=6-9). Scale bar = 500 μm. (D) Comparison of platelet counts between baseline, day 3, and day 9 post-injury in each mouse strain. Sample numbers (n) at baseline = 10, day 3 post-injury = 6-9, and day 9 post-injury = 10-13, respectively. *$**p<0.01$*. (E) Immunofluorescence staining of CD31 (green) in unchallenged skin of WT and genetically modified mice (n=5). Hoechst counterstains nuclei (blue). Scale bar = 50 μm. (F) Immunohistochemistry staining shows podoplanin (brown) on lymphatic vessels in unchallenged skin of WT and genetically modified mice (n=5). PDPN = podoplanin. Scale bar = 50 μm.

Figure S2

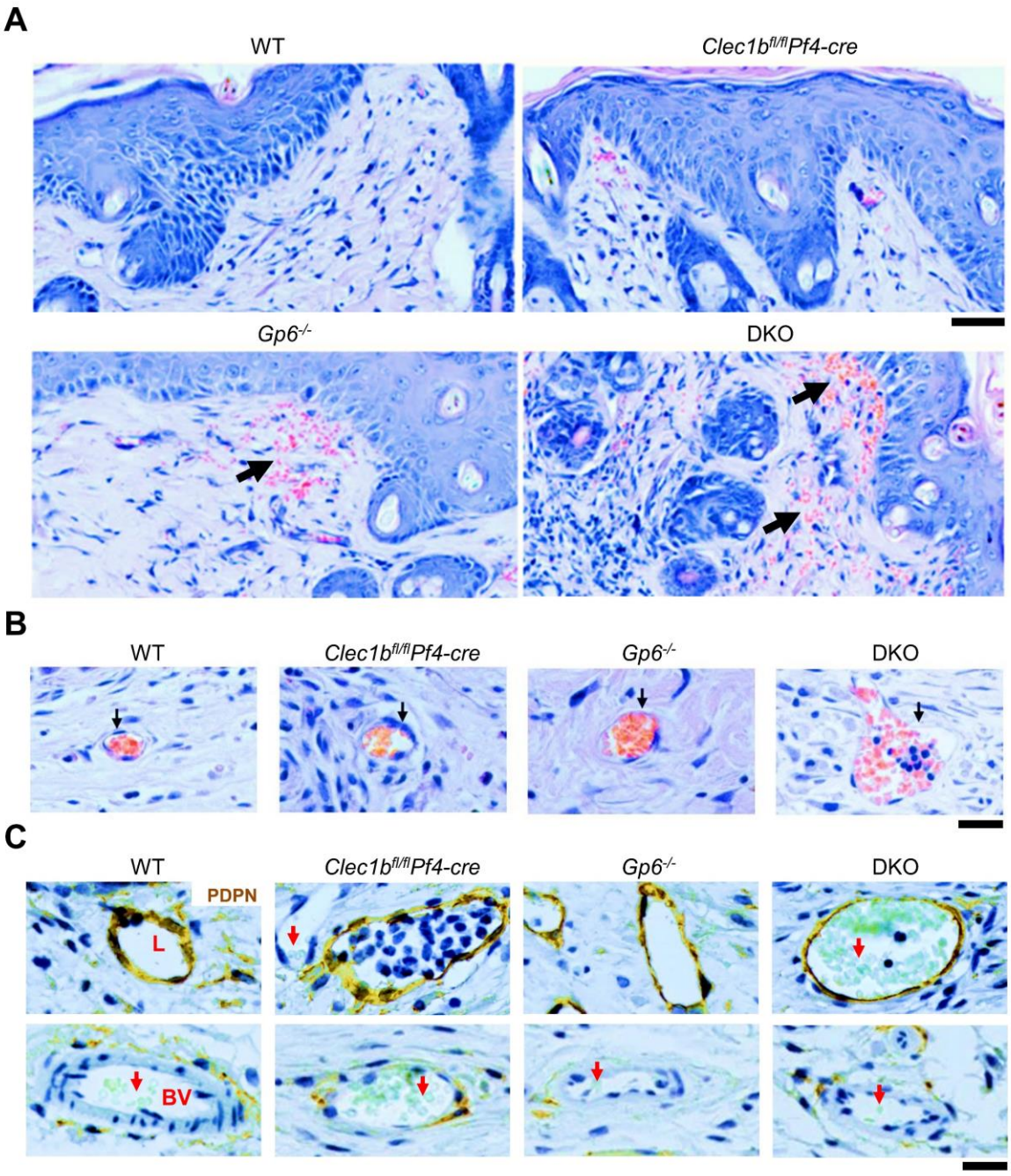
A
WT
Clec1b^fl/fl Pf4-cre
Gp6^-/-
DKO
B
WT
Clec1b^fl/fl Pf4-cre
Gp6^-/-
DKO
C
WT
Clec1b^fl/fl Pf4-cre
Gp6^-/-
DKO
PDPN
L
BV

Figure S2. Vascular leakage is observed in DKO mice and less marked in *Gp6*$^{-/-}$ mice during the inflammatory phase of wound healing. (A) H&E staining of wounds at day 3 post-injury (n=6-9). Arrow indicates bleeding into surrounding skin. Scale bar = 50 µm. (B) H&E staining of wound scar at day 9 post-injury (n=10-13). Arrow indicates red blood cells within the vessel. Scale bar = 20 µm. (C) Immunohistochemistry shows podoplanin on lymphatic endothelium (upper panel) and cells around blood vessel (lower panel). L = lymphatic vessel. BV = blood vessel. Arrow points to red blood cells in both types of vasculature. Scale bar = 20 µm.

Figure S3

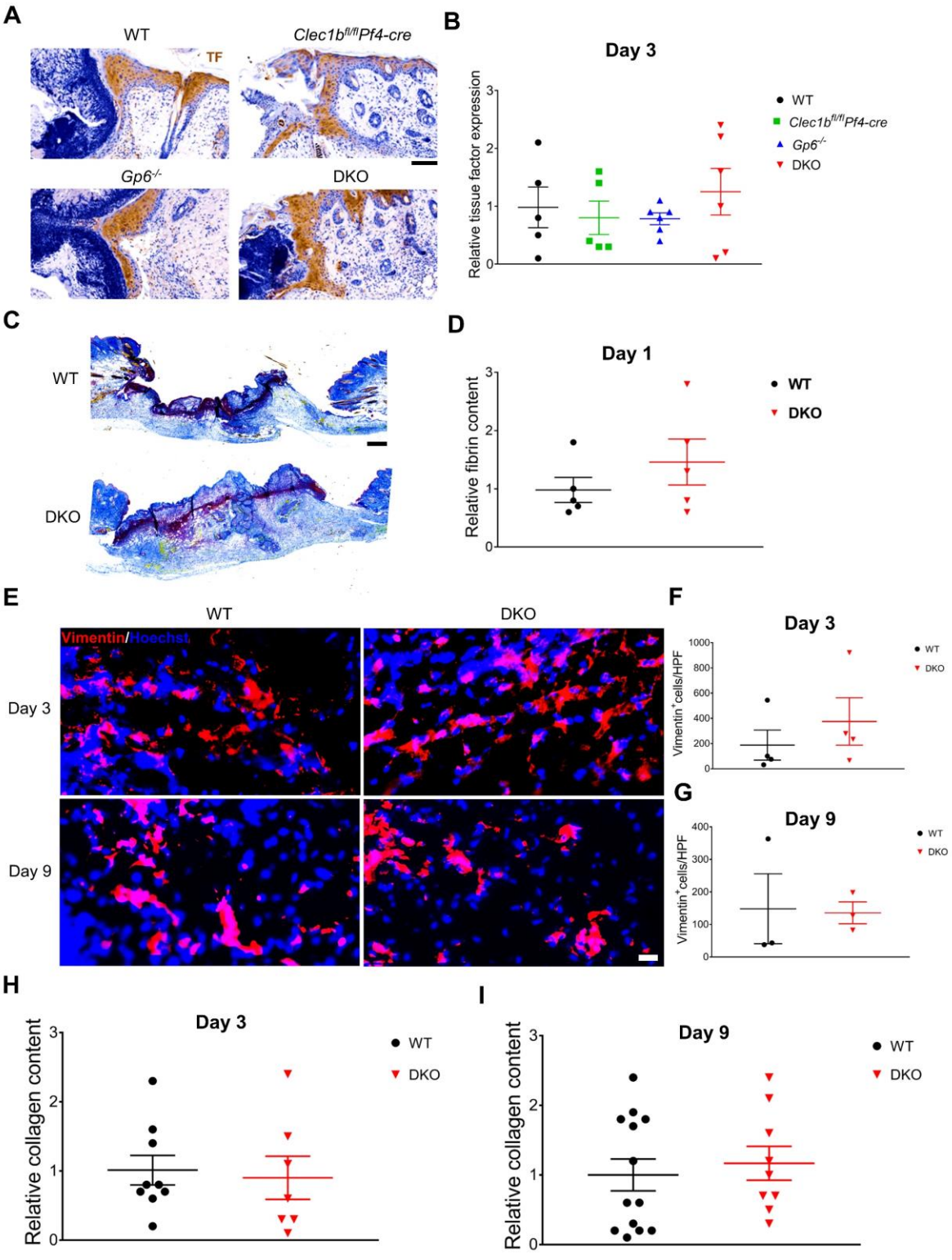
A
WT
Clec1b^fl/fl Pf4-cre
TF
Gp6^-/-
DKO
B
Day 3
Relative tissue factor expression
WT
Clec1b^fl/fl Pf4-cre
Gp6^-/-
DKO
C
WT
DKO
D
Day 1
Relative fibrin content
WT
DKO
E
WT
DKO
Vimentin/Hoechst
Day 3
Day 9
F
Day 3
Vimentin+cells/HPF
WT
DKO
G
Day 9
Vimentin+cells/HPF
WT
DKO
H
Day 3
Relative collagen content
WT
DKO
I
Day 9
Relative collagen content
WT
DKO

Figure S3. Normal TF, (myo)fibroblasts, and collagen content in DKO during the course of skin wound healing. (A) Immunohistochemistry staining of tissue factor (brown) at day 3 post-injury. TF = tissue factor. Scale bar = 50 μm. (B) Quantification of tissue factor at day 3 post-injury (n=5-6). (C) Martius scarlet blue (MSB) staining of skin wound at day 1 post-injury. Red = old fibrin, blue = collagen, yellow = red blood cells/fresh fibrin. Scale bar = 200 μm. (D) Quantification of fibrin content in the wound at day 1 post-injury (n=5). (E) Immunofluorescence staining of (myo)fibroblasts (vimentin$^+$ cells; red) in the wound of WT and DKO mice at day 3 (n=4) and day 9 post-injury (n=3). Hoechst counterstains nuclei (blue). Scale bar = 20 μm. (F) Quantification of (myo)fibroblasts (vimentin$^+$ cells) at day 3 post-injury (n=4). (G) Quantification of (myo)fibroblasts (vimentin$^+$ cells) at day 9 post-injury (n=3). (H) Quantification of collagen content (blue color) in MSB staining within the wound at day 3 post-injury (n=7-9). (I) Quantification of collagen content within the scar at day 9 post-injury (n=9-13). Graphs are presented as mean ± SEM and analyzed by either one-way ANOVA with Bonferroni's multiple comparison test (B) or Student's t-test (D, F, G, H, and I).

Figure S4

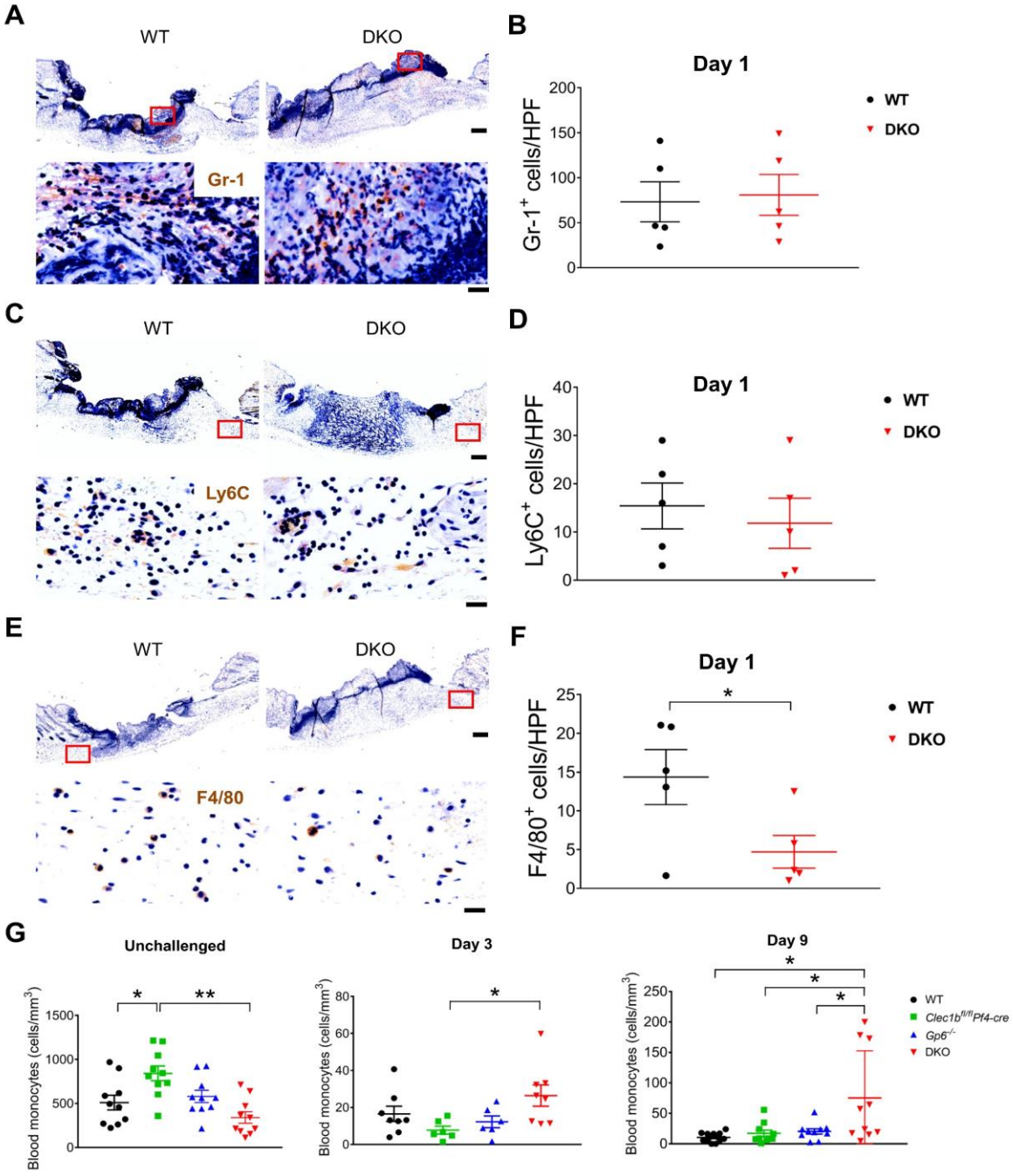
A
WT
DKO
Gr-1
B
Day 1
Gr-1+ cells/HPF
WT
DKO
C
WT
DKO
Ly6C
D
Day 1
Ly6C+ cells/HPF
WT
DKO
E
WT
DKO
F4/80
F
Day 1
F4/80+ cells/HPF
WT
DKO
G
Unchallenged
Day 3
Day 9
Blood monocytes (cells/mm3)
WT
Clec1bfl/flPf4-cre
Gp6-/-
DKO

Figure S4. Wound neutrophils and monocytes are unaltered but macrophage influx is decreased in DKO mice at day 1 post-injury. (A) Staining of neutrophils (Gr-1; brown) in wound area at day 1 post-injury. (B) Quantification of neutrophils (Gr-1^+ cells) in wound area at day 1 post-injury (n=5). (C) Staining of monocytes ($Ly6C^+$; brown) in wound area at day 1 post-injury. (D) Quantification of monocytes ($Ly6C^+$ cells) in wound area at day 1 post-injury (n=5). (E) Detection of macrophages (F4/80 staining; brown) in wound area at day 1 post-injury. (F) Quantification of macrophages ($F4/80^+$ cells) in wound area at day 1 post-injury (n=5). (G) Comparison of blood monocytes between all groups at baseline (left), day 3 (middle), and day 9 post-injury (right). Graphs are presented as mean ± SEM and analyzed by either Student's t-test (B, D, and F) or one-way ANOVA with Bonferroni's multiple comparison test (G). *$p<0.05$, **$p<0.01$*. Scale bar = 200 μm (upper panel), and 20 μm (lower panel).

Figure S5

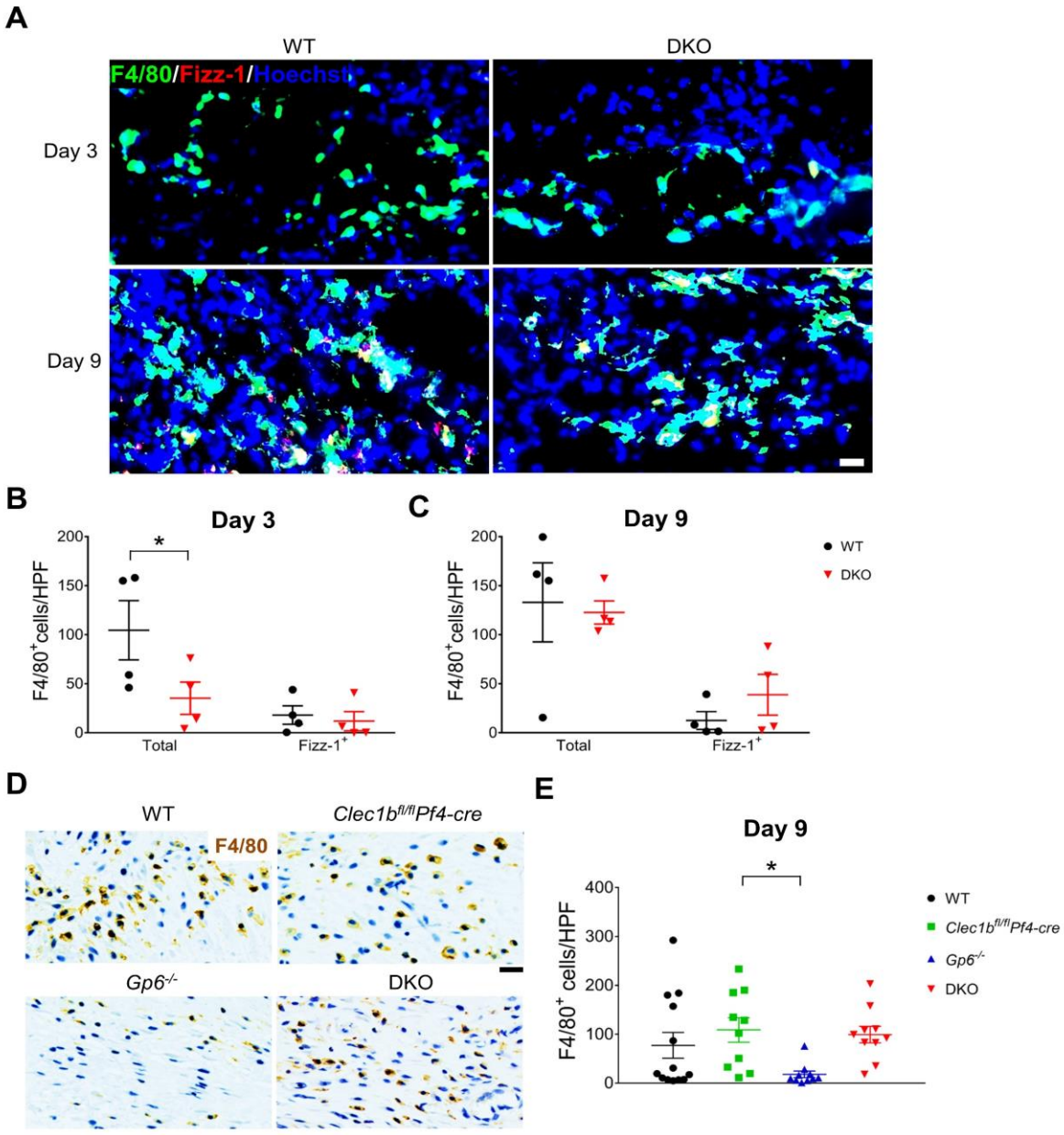
A
WT
DKO
F4/80/Fizz-1/Hoechst
Day 3
Day 9
B
Day 3
F4/80+cells/HPF
Total
Fizz-1+
C
Day 9
WT
DKO
D
WT
Clec1bfl/flPf4-cre
F4/80
Gp6-/-
DKO
E
Day 9
WT
Clec1bfl/flPf4-cre
Gp6-/-
DKO

Figure S5. Normal M2 macrophage recruitment in DKO mice during the course of wound healing. (A) Immunofluorescence double staining of Fizz-1 (red) and F4/80 (green) in the wound of WT and DKO mice at day 3 (n=4) and day 9 post-injury (n=4). Hoechst counterstains nuclei (blue). Scale bar = 20 µm. (B) Quantification of M2 macrophages (Fizz-1^{+}F4/80^{+} cells; yellow) at day 3 post-injury (n=4). (C) Quantification of M2 macrophages (Fizz-1^{+}F4/80^{+} cells; yellow) at day 9 post-injury (n=4). (D) Detection of F4/80^{+} cells (brown) in wound at day 9 post-injury. Scale bar = 20 µm. (E) Quantification of F4/80^{+} cells in wound at day 9 post-injury (n=10-13). Graphs are presented as mean ± SEM and analyzed by either Student's t-test (B and C) or one-way ANOVA with Bonferroni's multiple comparison test (E). *$p < 0.05$.

Figure S6

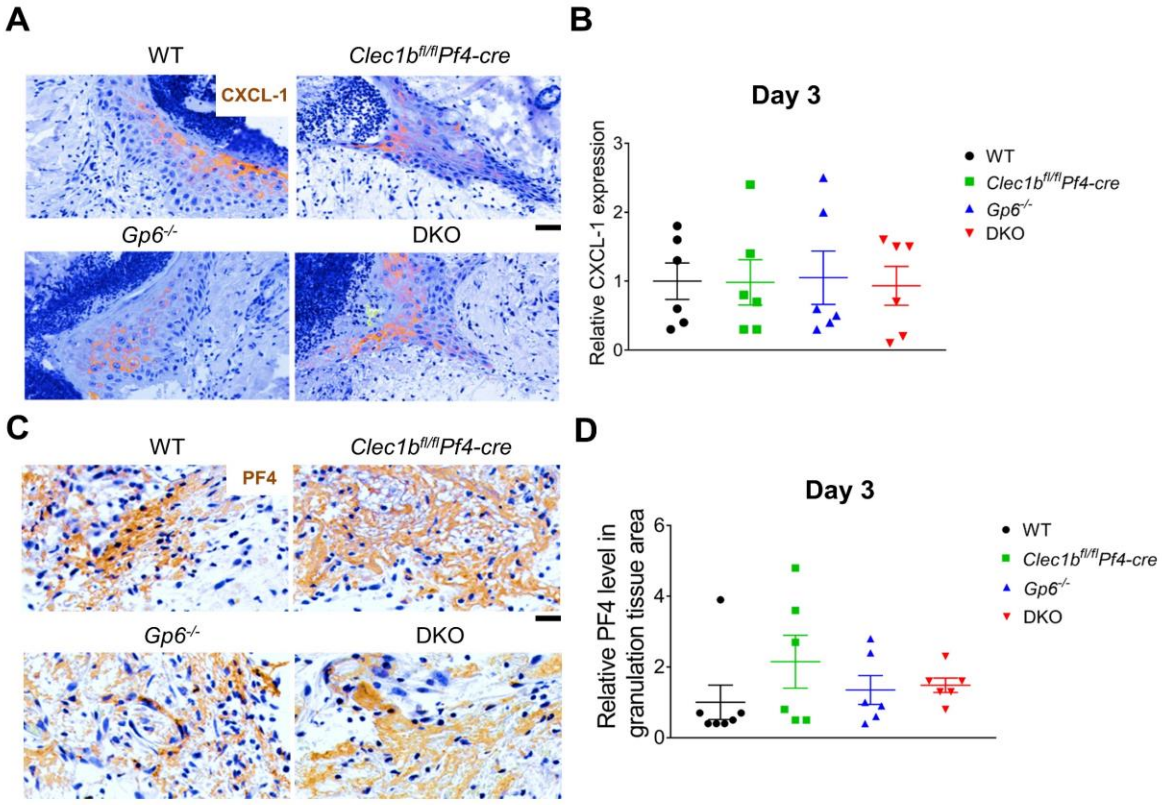

Figure S6. Normal expression of CXCL-1 and PF-4 at day 3 post-injury in DKO mice. (A) Detection of CXCL-1 (brown) in wound area at day 3 post-injury. (B) Quantification of keratinocyte-expressed CXCL-1 in wound area at day 3 post-injury (n=6). (C) Detection of PF4 (brown) in wound area at day 3 post-injury. (D) Quantification of PF4 within the granulation tissue in wound area at day 3 post-injury (n=6). Data are presented as mean ± SEM and analyzed by one-way ANOVA with Bonferroni's multiple comparison test. Scale bar = 20 μm.

Figure S7

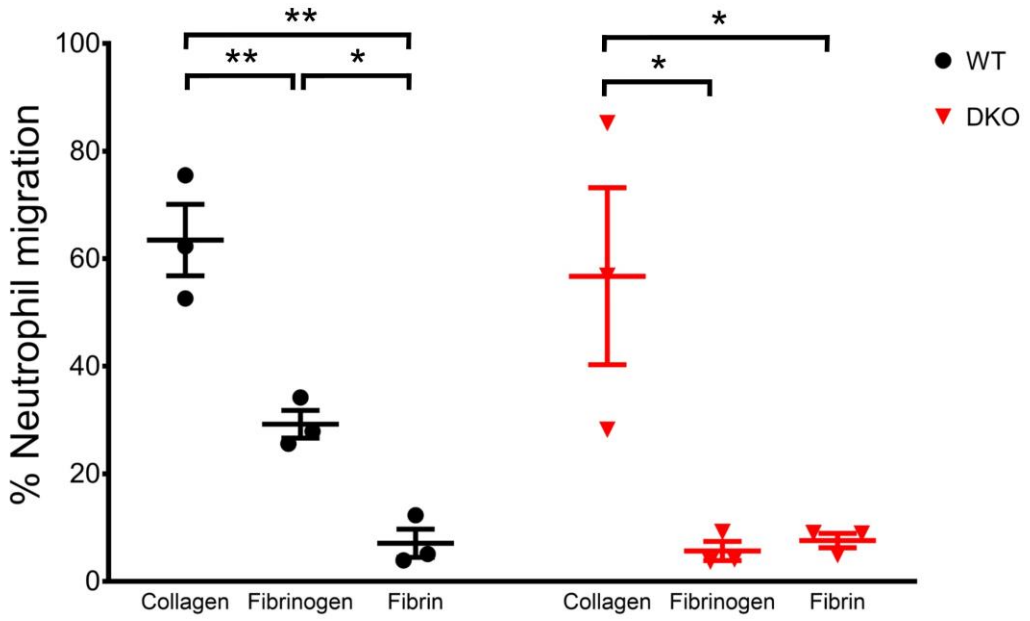

Figure S7. Fibrinogen and crosslinked fibrin matrix attenuate neutrophil chemotaxis *in vitro*. Graphs represent migration of neutrophils through collagen, fibrinogen, and fibrin matrix (n=3). Data are presented as mean ± SEM and analyzed by one-way ANOVA. **p<0.05, **p<0.01.*

Figure S8

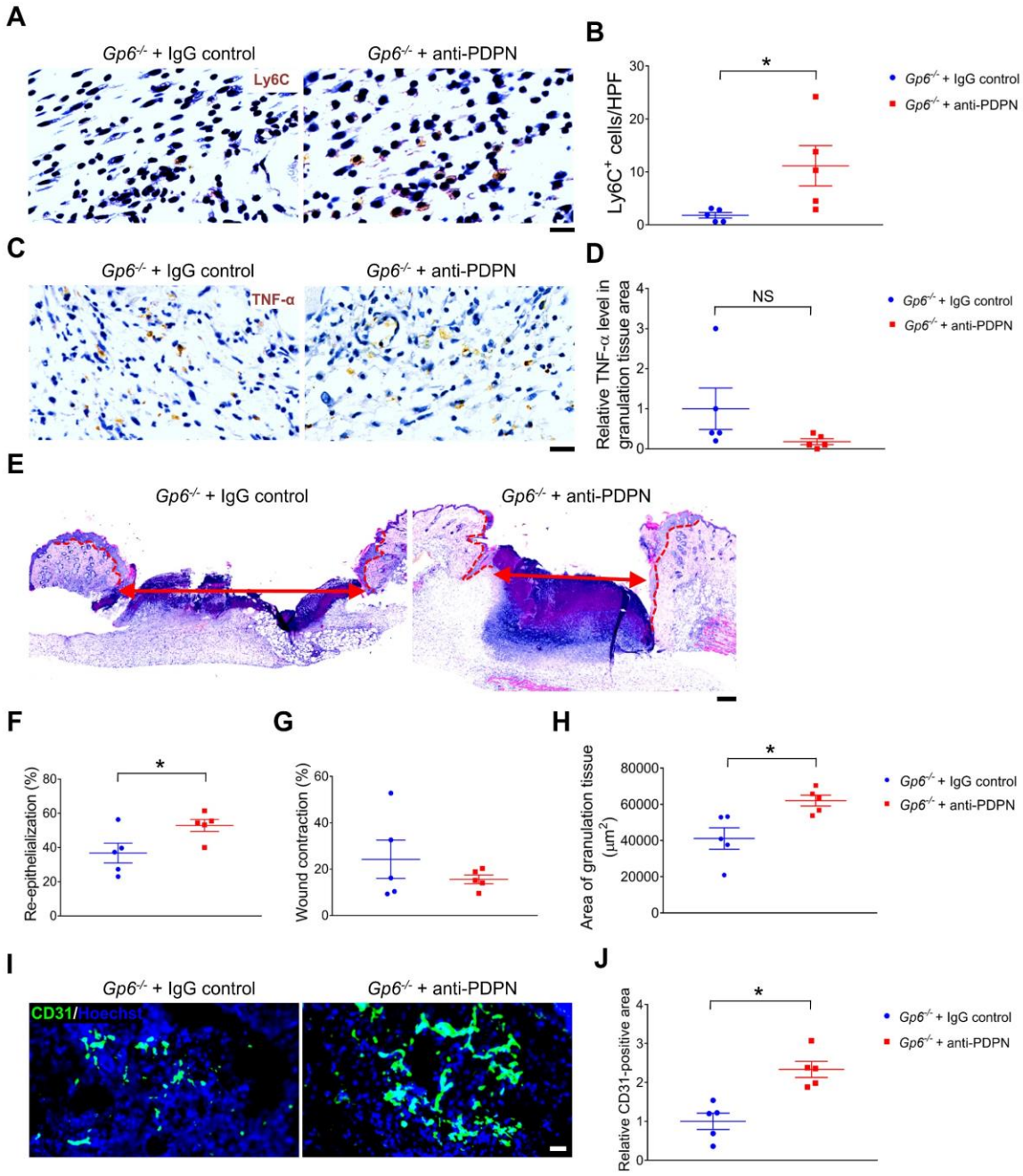
A
Gp6-/- + IgG control
Gp6-/- + anti-PDPN
Ly6C
B
Ly6C+ cells/HPF
Gp6-/- + IgG control
Gp6-/- + anti-PDPN
C
TNF-α
D
Relative TNF-α level in granulation tissue area
NS
E
F
Re-epithelialization (%)
G
Wound contraction (%)
H
Area of granulation tissue (μm2)
I
CD31/Hoechst
J
Relative CD31-positive area

Figure S8. Increased wound monocytes, enhanced angiogenesis, rapid re-epithelialization and greater granulation tissue formation in *Gp6*$^{-/-}$ mice treated with anti-podoplanin antibody. (A) Detection of Ly6C^{+} cells (brown) in wound at day 3 post-injury. Scale bar = 20 μm. (B) Quantification of Ly6C^{+} cells in wound at day 3 post-injury (n=5). (C) Immunohistochemistry staining of TNF-α (brown) in the wound at day 3 post-injury. Scale bar = 20 μm. (D) Quantification of TNF-α level in granulation tissue area at day 3 post-injury (n=5). (E) H&E staining at day 3 post-injury. Dotted line indicates hyperplastic coverages. Arrow indicates gap between epithelial tongues. Scale bar = 500 μm. (F) Measurement of re-epithelialization (n=5). (G) Measurement of wound contraction (n=5). (H) Quantification of granulation tissue area (n=5). (I) Immunofluorescence staining of endothelial cells (CD31^{+} cells; green) in wound area at day 3 post-injury. Hoechst counterstains nuclei (blue). Scale bar = 50 μm. (J) Quantification of CD31^{+} area within the wound at day 3 post-injury (n=5). All graphs are presented as mean ± SEM and analyzed by Student's t-test. *$p<0.05$. NS = non-significant.

Figure S9

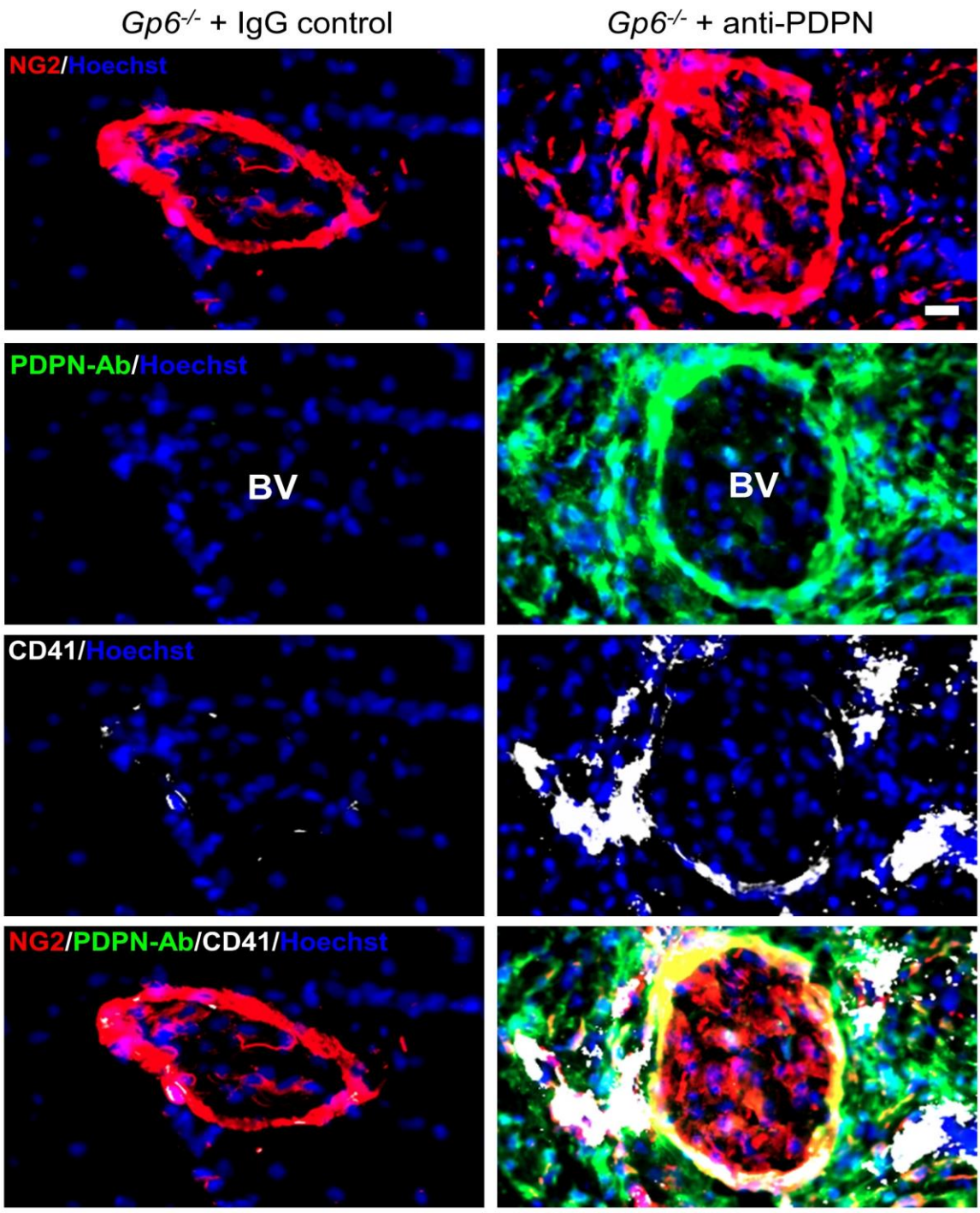
Gp6-/- + IgG control
Gp6-/- + anti-PDPN
NG2/Hoechst
PDPN-Ab/Hoechst
BV
BV
CD41/Hoechst
NG2/PDPN-Ab/CD41/Hoechst

Figure S9. Anti-podoplanin antibody (PDPN-Ab) is detected together with extravascular platelets at perivascular area in *Gp6*$^{-/-}$ mice treated with this antibody. Immunofluorescence staining of NG2 (red), PDPN-Ab (green) and CD41 (white) illustrates extravasation of platelets and the presence of PDPN-Ab on pericytes (NG2^{+}) and other cells around blood vessel at day 3 after injury (n=4-5). Alexa 488-conjugated goat anti-hamster IgG secondary antibody was used in immunofluorescence to detect the injected PDPN-Ab (clone 8.1.1.). Hoechst counterstains nuclei (blue). BV = blood vessel. Scale bar = 20 µm.

Figure S10

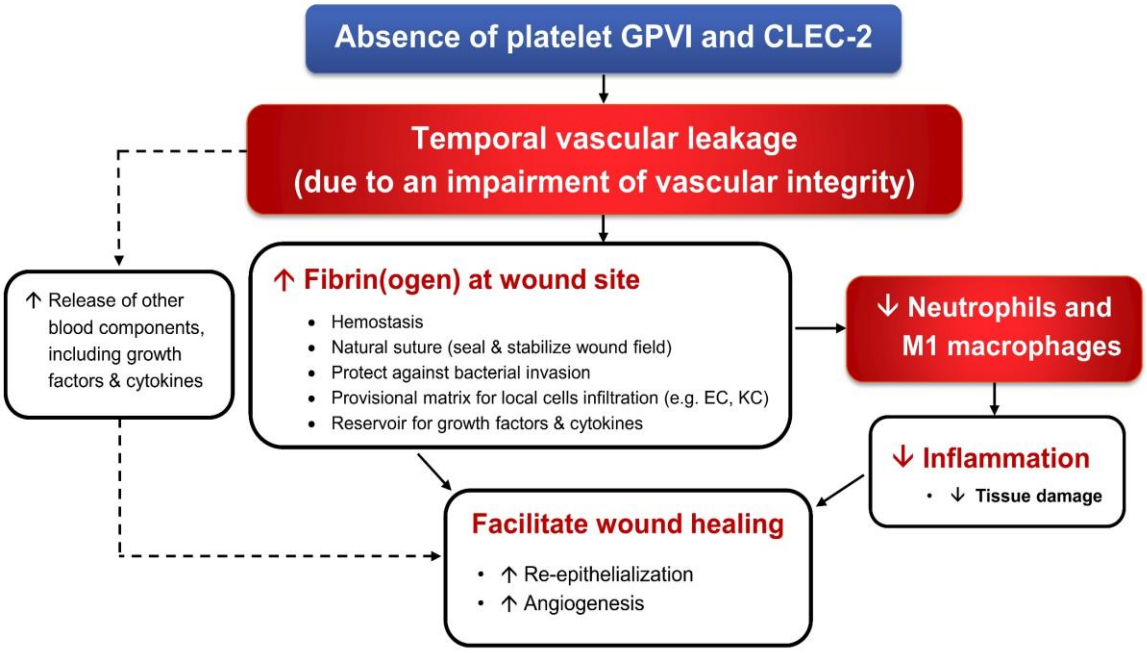

Figure S10. Schematic illustration for multifactorial contribution of accelerated skin wound healing in the absence of platelet ITAM receptors. A lack of GPVI and CLEC-2 results in transient vascular leakage, which contributes to higher fibrin(ogen) content at wound site. In addition, plasma-derived macromolecules (e.g. clotting factors, growth factors, and cytokines) may also leak into the wound. Moreover, ITAM-receptor deficiency decreases wound leukocytes during inflammatory phase, likely because of a physical blockade by fibrin(ogen) and a decrease in neutrophil capacity to migrate through fibrinogen, which subsequently attenuates inflammation and tissue damage. These two mechanisms associate with an accelerated skin wound healing, at least by facilitating re-epithelialization and angiogenesis. EC = endothelial cells, KC = keratinocytes.